Deep Circulation in the South Atlantic Induced by Bottom-Intensified Mixing over the Midocean Ridge*

RUI XIN HUANG AND XIANGZE JIN

Department of Physical Oceanography, Woods Hole Oceanographic Institution, Woods Hole, Massachusetts

(Manuscript received 4 April 2001, in final form 23 August 2001)

ABSTRACT

The deep circulation in the South Atlantic is studied through numerical experiments, using an oceanic general circulation model based on *z* coordinates. The new feature of these numerical experiments is that diapycnal mixing is idealized as strong bottom-intensified mixing on both sides of the midocean ridge; elsewhere diapycnal mixing is set at a low background value.

The bottom-intensified diapycnal mixing induces strong equatorward (poleward) flow along the western (eastern) slope of the midocean ridge. In addition, the strong vertical gradient of diapycnal mixing rate induces downwelling in the basin interior and intensifies the upwelling near the axis of the midocean ridge. The strong ridge-following currents induce anticlockwise circulation in both the eastern and western deep basins, and such circulation is opposite to the classical Stommel–Arons circulation. This study indicates that bottom topography, strong mixing over the midocean ridge, and strong localized mixing associated with overflows can have major impact on the strength of the deep meridional overturning cell and deep water properties in the whole deep basin.

1. Introduction

The general circulation of the ocean plays a vitally important role in the global environment, especially the climate. Among many competing physical processes, diapycnal mixing has been identified as one of the most important controlling factors. For the case of a uniform mixing rate, it is well known that the meridional overturning rate increases if mixing is enhanced (Bryan 1987). Although mixing is very important in controlling the circulation, the physical processes involved are very complicated; therefore, our understanding of mixing processes in the oceans remains rather rudimentary.

Most previous theoretical and numerical studies have been based on the assumption of a spatially uniform rate of mixing (e.g., Bryan 1987). The dynamic consequence of nonuniform mixing has been explored by some investigators. For example, Bryan and Lewis (1979) carried out numerical experiments in which the mixing rate in the deep ocean is assumed to be higher than in the upper oceans. More recently, several investigators explored the consequences of a strongly nonuniform rate of mixing (e.g., Marotzke 1997; Samelson 1998). These authors studied the circulation driven by strong mixing confined to either the western or eastern boundaries of a square basin without bottom topography.

Although these studies shed light on the circulation driven by nonuniform mixing, some of the most important questions related to the circulation in the deep ocean have not been answered, such as the dynamic roles of bottom topography and of strong mixing near the midocean ridge.

The theory of deep circulation was first proposed by Stommel and Arons (1960). In their theory, it was assumed that deep circulation is driven by uniform upwelling fed by point sources of deep water that are confined to several isolated places in the world oceans. Without considering bottom topography, they came to a simple circulation pattern, including poleward flow in the ocean interior and western boundary currents. Since their model included neither the role of mixing nor that of dissipation, the circulation could be readily derived from a simple linear vorticity balance. In a similar way, the deep circulation can be inferred from the vorticity balance if one assumes some simple forms of vorticity dissipation. In a recent study, Yang and Price (2000) extended the classical theory of Stommel and Arons by invoking a simple form of bottom drag and vertical velocity field.

Although these theories provide us with some possible patterns for the deep circulation under the specific assumptions, they may not necessarily give us realistic

* Woods Hole Oceanographic Institution Contribution Number 10476.

Corresponding author address: Dr. Rui Xin Huang, MS 21, Woods Hole Oceanographic Institution, Woods Hole, MA 02543.
E-mail: rhuang@whoi.edu

solutions to the world oceans. The fundamental difficulties in revealing the deep circulation are related to the complicated spatial patterns of mixing and the intimate connection between circulation, mixing, and bottom topography.

Flow induced by bottom-intensified mixing over sloping boundaries has been studied extensively over the past several decades. Phillips (1970) and Wunsch (1970) pointed out that a thermal insulation boundary condition applied to a sloping bottom requires that isotherms must be perpendicular to the local slope. In a rotating fluid such a density gradient near the bottom boundary thus induces an alongslope flow (the primary circulation) and an uphill flow (the secondary circulation) in the bottom boundary layer. These currents have been studied by many investigators. For example, Thompson and Johnson (1996) carried out numerical simulations for currents generated by diffusion and geothermal heating over bottom slope, with a time-dependent two-dimensional model. Phillips et al. (1986) also showed that a tertiary flow perpendicular to the slope may exist due to the convergence and divergence of the secondary circulation. For the comprehensive review the reader is referred to papers by Garrett (1991) and Garrett et al. (1993).

Recently, Cummins and Foreman (1998) studied the circulation induced by bottom-intensified mixing over a seamount. The most important result from their study is the existence of an anticyclonic circulation around the seamount, the uphill flow over the slope, and a tertiary circulation. As will be shown in our study, the circulation in the deep basin, such as the Brazil and Angola Basins, has a similar structure. Some simple theoretical studies, such as those by Spall (2001), also have been carried out in order to explore the circulation induced by bottom-intensified mixing.

The deep circulation in the South Atlantic has been discussed in many papers, for example, Hogg et al. (1982, 1996), Hogg and Owens (1999), De Madron and Weatherly (1994), and Warren and Speer (1991). In this study we will focus on the deep circulation in the Brazil Basin and the Angola Basin, using a numerical model. It seems likely that substantial progress in understanding the mixing in the ocean may happen within the next 5 to 10 years; however, we do not currently have a very reliable way of parameterizing the mixing. Thus, in this study our approach is based on assuming a rather simple formula. Although such a formula may oversimplify the mixing process in the ocean, we hope such a study may provide us with some useful insight into the physics. Specifically, our formulation is based on a given pattern of mixing rate that is especially strong over the midocean ridge, suggested by recent field observations (Polzin et al. 1997). Our goal here is to explore the dynamic consequences of the bottom-intensified mixing over the midocean ridge, while the exact nature and its parameterization of such a mixing pattern will be left for further studies. The model is formulated in section 2, and the numerical results for the South Atlantic are discussed in section 3, with conclusions in section 4.

2. Model formulation

Our numerical model is based on the Geophysical Fluid Dynamics Laboratory (GFDL) Modular Ocean Model, version 2 (MOM2) (Pacanowsky 1995). The model is based on z coordinates, including the recent development of mixing tensor rotation into the isopycnal and diapycnal directions, plus on eddy-induced tracer advection. Most previous studies have been based on rather low vertical resolution in the deep ocean. Recently, there has been much effort in improving the simulation of the deep circulation in z-coordinates models, such as using the fractional thickness or fractional volume technique, and the addition of a bottom boundary layer (e.g., Song and Chao 2000). In this study, however, we will attempt to improve the simulation by using a large number of layers: 110 layers, each of uniform thickness 50 m. Our motivation in using such a fine vertical resolution is to make sure that the model will be able to resolve the bottom boundary layer adequately. We are aware of the limitations of our model formulation. For example, there is spurious diapycnal mixing associated with the advection terms in a z-coordinate model, as discussed by Griffies et al. (2000). Therefore, the actual distribution of diapycnal mixing in the numerical model is somehow different from what we specified. However, this is our first step toward understanding the circulation driven by highly nonuniform mixing, so a lot of questions are left for further studies.

The new feature of our model is the inclusion of strong diapycnal mixing over both sides of the midocean ridge. Recent field observations (Polzin et al. 1997; Ledwell et al. 2000) indicate that mixing is very strong in the eastern half of the Brazil Basin, but it is very weak in the western half. Thus, we will idealize the mixing in the model ocean by the following recipe:

$$\kappa = \kappa_0 + \Delta\kappa_1 \exp\left[-\left(\frac{z + h}{\Delta h}\right)^2\right] \qquad (1)$$

where $\kappa_0 = 10^{-5}$ m^2 s^{-1} is the low background mixing rate, $\Delta\kappa_1 = 10^{-3}$ m^2 s^{-1} is the strong bottom-intensified mixing on both sides of the midocean ridge, h is the depth of the ocean, and $\Delta h = 600$ m is the e-folding distance of the bottom-intensified mixing. As discussed above, $\Delta\kappa_1$ is set to zero for the western half of the Brazil Basin and the eastern half of the Angola Basin.

Our model geometry is based on the real topography and coastline of the South Atlantic, from 41°S to 6°N with a resolution of 1° × 1° (Fig. 1). The subgrid-scale mixing parameterization is 1) the horizontal and vertical momentum mixing coefficients are $A_m = 10^4$ m^2 s^{-1} and $A_v = 10^{-4}$ m^2 s^{-1}, 2) the along-isopycnal mixing rate and the eddy-induced transport coefficient are

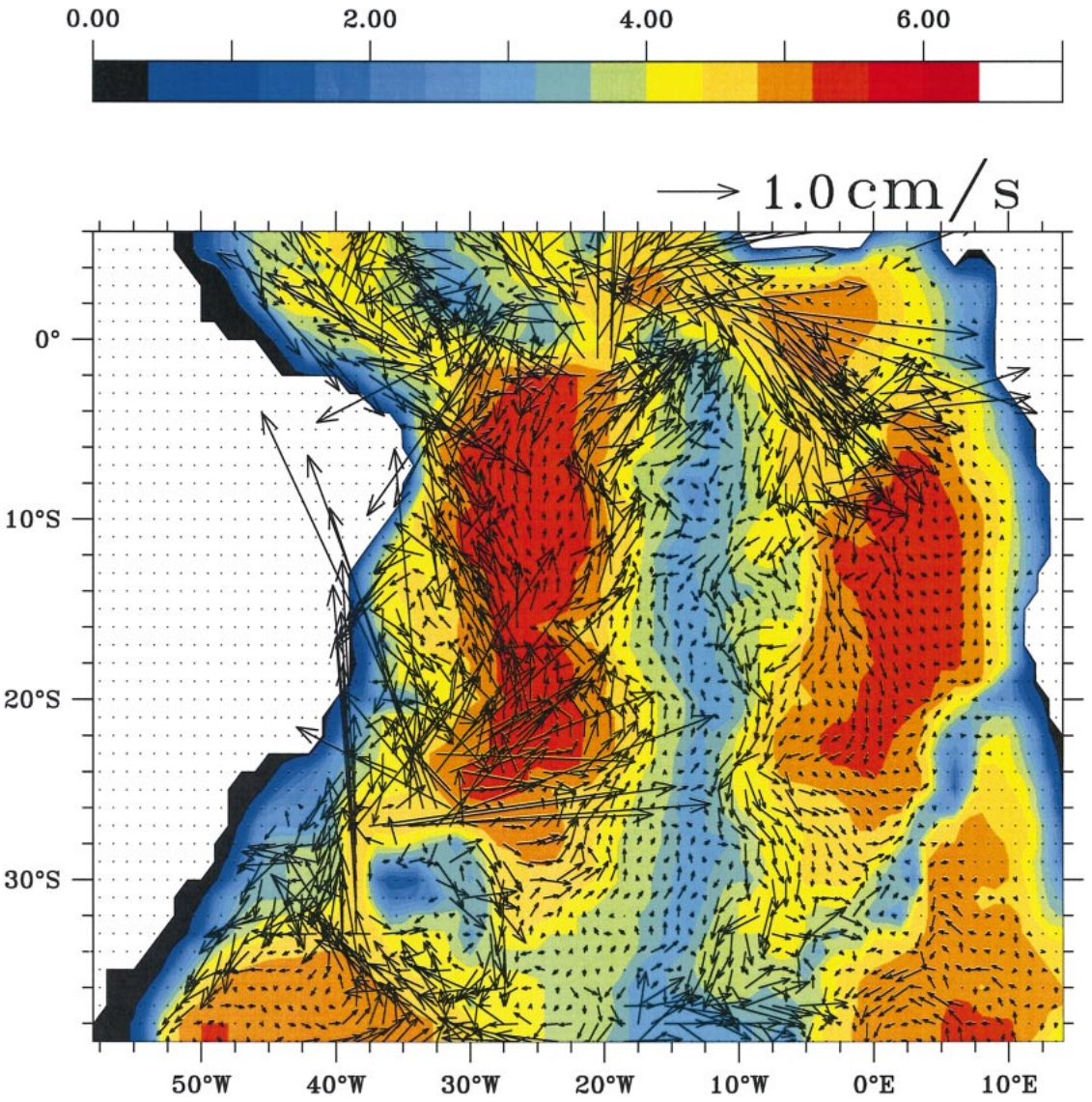

FIG. 1. The topography (km) and horizontal velocity in bottom boxes deeper than 3 km (case A) for the model South Atlantic.

$k_h = 10^3$ m^2 s^{-1}, and 3) diapycnal mixing rate k_v varies as described earlier.

Our study is focused on a model for the South Atlantic with a horizontal resolution of 1° × 1°. The model is forced by the monthly-mean wind stress of Hellerman and Rosenstein (1983) and sea surface temperature and salinity relaxation to the monthly mean climatology (Levitus and Boyer 1994; Levitus et al. 1994). The northern (southern) boundary is set along 6°N (41°S) where a sponge layer is used in which the model's thermodynamic variables are relaxed back to the climatology.

Due to the low horizontal resolution, the Vema Channel cannot be fully resolved, so we have artificially ''dug'' a channel (4600 m, near 30°S, 39°W) in our model to insure that Antarctic Bottom Water (AABW) can flow into the Brazil Basin at the right depth. Similarly, we treat the Romanche Fracture Zone with care by digging a channel 4350 m deep (around 19°W near the equator); thus, the communication of AABW through the southern end of the Brazil Basin and its further communication to the Angola Basin is simulated by channels of appropriate depth. The topography is shown in Fig. 1.

Using this topography, we carried out four numerical experiments. In case A, a bottom-intensified diapycnal mixing applied to both sides of the midocean ridge, with the boundary between strong mixing and background weak mixing set along a ''meridional'' line that follows the maximum depth of the sub-basins on both sides of the midocean ridge.

For comparison, we also carried out two additional

experiments with uniform mixing rate: In case B, the mixing rate was set to the background value of $\kappa = 10^{-5}$ m^2 s^{-1} and, in case C, the mixing rate was set to $\overline{\kappa} = 0.8451 \times 10^{-4}$ m^2 s^{-1}, the basin-mean mixing rate for case A. In comparison, the basin-average diapycnal mixing rate for Antarctic Bottom Water is estimated as $\overline{\kappa} \approx 1$–5 ($\times 10^{-4}$ m^2 s^{-1}) (Hogg et al. 1982; Morris et al. 2001).

After the completion of cases A, B, and C, it was found that bottom water in the Angola Basin is much colder than observations, a clear sign that mixing for water in the Angola Basin is not strong enough. Although we do not really know much about the mixing rate in the Angola Basin, a very likely cause of such a problem is that mixing in the Romanche Fracture Zone is too weak, compared with observations. As reported by Polzin et al. (1996) and Ferron et al. (1998), the mixing rate can be as large as 0.1 m^2 s^{-1} within the Romanche Fracture Zone, where water drops over more than 500 m within 100 km of downward flow. In order to explore the dynamical effects of such strongly localized mixing, we carried out a fourth numerical experiment (case D) as follows.

A strongly localized mixing was placed near the Romanche Fracture Zone, that is,

$$\kappa = \kappa_0 + (\Delta\kappa_1 + \Delta\kappa_2) \exp\left[-\left(\frac{z + h}{\Delta h}\right)^2\right] \quad (2)$$

$$\Delta\kappa_2 = \Delta\kappa \exp\left[-\frac{(x - x_0)^2 + (y - y_0)^2}{D^2}\right] \quad (3)$$

where $\Delta\kappa = 0.1$ m^2 s^{-1} and $D = 200$ km. In case D we chose $\Delta\kappa_1 = 1 \times 10^{-3}$ m^2 s^{-1}.

3. Numerical results

All these numerical experiments started from the initial state of an ocean at rest with the annual mean temperature and salinity adapted from the Levitus climatology. The model is forced by climatological wind stress and relaxation to climatological sea surface temperature and salinity, and integrated 250 years for each case. The volume flux of the AABW into the Brazil Basin is estimated as 4 Sv (Sv $\equiv 10^6$ m^3 s^{-1}) (Hogg et al. 1982), so the renewal time for the water mass is about 100 years. Thus, a 250-yr numerical experiment should be long enough to reach quasi equilibrium under the relaxation conditions along both the northern and southern boundaries. The seasonal cycle in properties at deep levels is not the focus of this study; thus, the results discussed below are based on the annual mean.

a. The horizontal velocity field

The most prominent feature of the circulation is the strong bottom current near the midocean ridge in case A (Fig. 1). In the Brazil Basin, there is strong bottom current along the western slope of the midocean ridge, which is almost as strong as the deep western boundary current along the western boundary of the basin. In general the flow on the seafloor is equatorward. Bottom water enters the Angola Basin in forms of a relatively strong western boundary current along the eastern slope of the midocean ridge, and the circulation in the basin interior is anticlockwise. Thus, deep circulations in both the Brazil Basin and Angola Basin are opposite to the direction predicted by Stommel and Arons (1960).

In the Brazil Basin there are western boundary currents flowing along the eastern coast of South America, as seen in the horizontal velocity diagram in Fig. 2. Over the upper 1.5 km, the surface western boundary current flows northward (Fig. 2a). This surface western boundary current is due to both the wind-driven circulation in the upper layer and the northward branch of the meridional thermohaline overturning cell.

For the depth range from 2 to 3.5 km, the western boundary current flows southward, carrying North Atlantic Intermediate Water and North Atlantic Deep Water (Fig. 2b). Around the depth of 4 km, the western boundary current switches to northward, carrying the Antarctic Bottom Water into the South and North Atlantic (Figs. 2c,d).

The dynamic effect of bottom-intensified mixing over the midocean ridge is not clear at depths shallower than the tip of the midocean ridge, which is around 3 km; however, at the depth of 4.5 and 5 km, the influence is very strong. For case A with strong bottom-intensified mixing over the ridge, there is a strong equatorward flow along the western slope of the midocean ridge (Fig. 2c). In fact, at the 4.5-km level, the eastern boundary current and the western boundary current in the Brazil Basin have roughly the same strength, with horizontal velocity on the order of 1 cm s^{-1}. The equatorward flow along the western slope of the midocean ridge is not inconsistent with the tracer field observations. Although the center of the tracer moves southwestward, there is a tail that moves equatorward along the western slope of the midocean ridge (see Fig. 1b in Ledwell et al. 2000). In the deep basin interior, flow is southward at the 4.5-km level, but it is mostly eastward at the 5-km level.

Therefore, the circulation is quite different from the classical Stommel–Arons theory. The departure from the Stommel–Arons theory is expected because the circulation in the deep basin is strongly constrained by both topography and the bottom-intensified mixing, which were absent in the original Stommel–Arons theory. In comparison, the horizontal velocity patterns obtained for cases B and C have similar structure; however, the eastern boundary current developed over the western slope of the midocean ridge is much weaker. A clear comparison can be made between cases A and C, shown in Figs. 2 and 3. Although the diapycnal mixing in case C is the same as the average rate in case A, the equatorward current along the western slope of the midocean

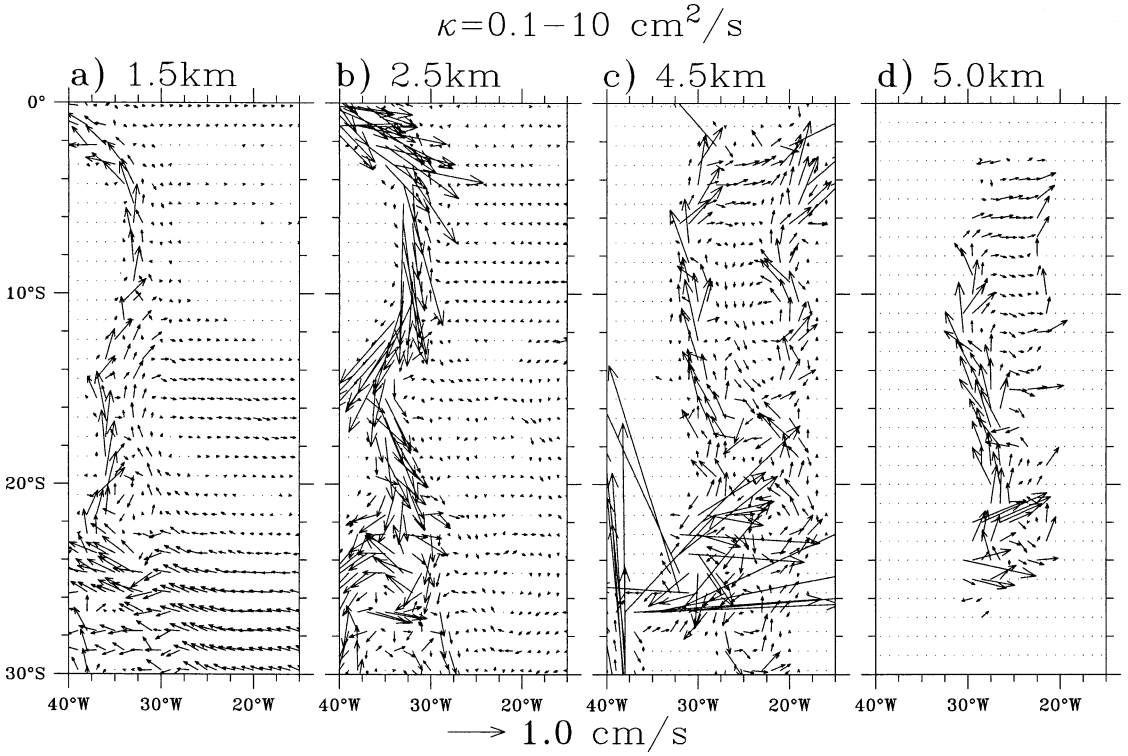

FIG. 2. Horizontal velocity within the Brazil Basin at different levels for case A.

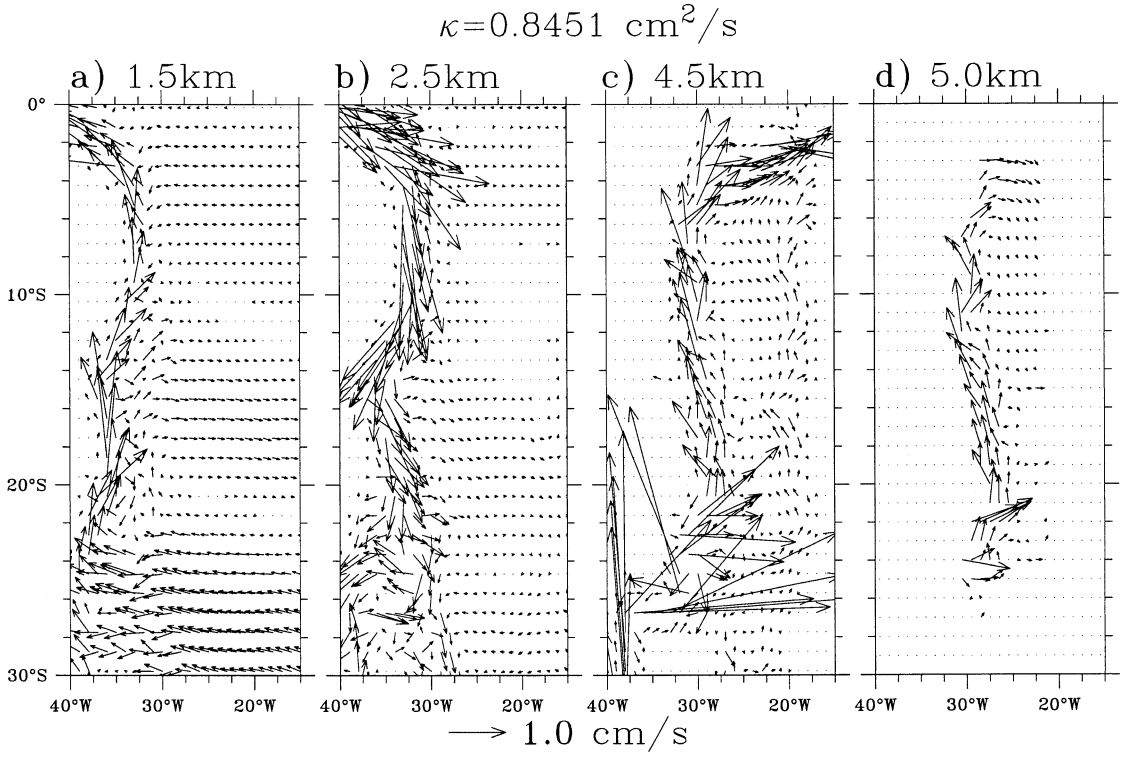

FIG. 3. Horizontal velocity within the Brazil Basin at different levels for case C.

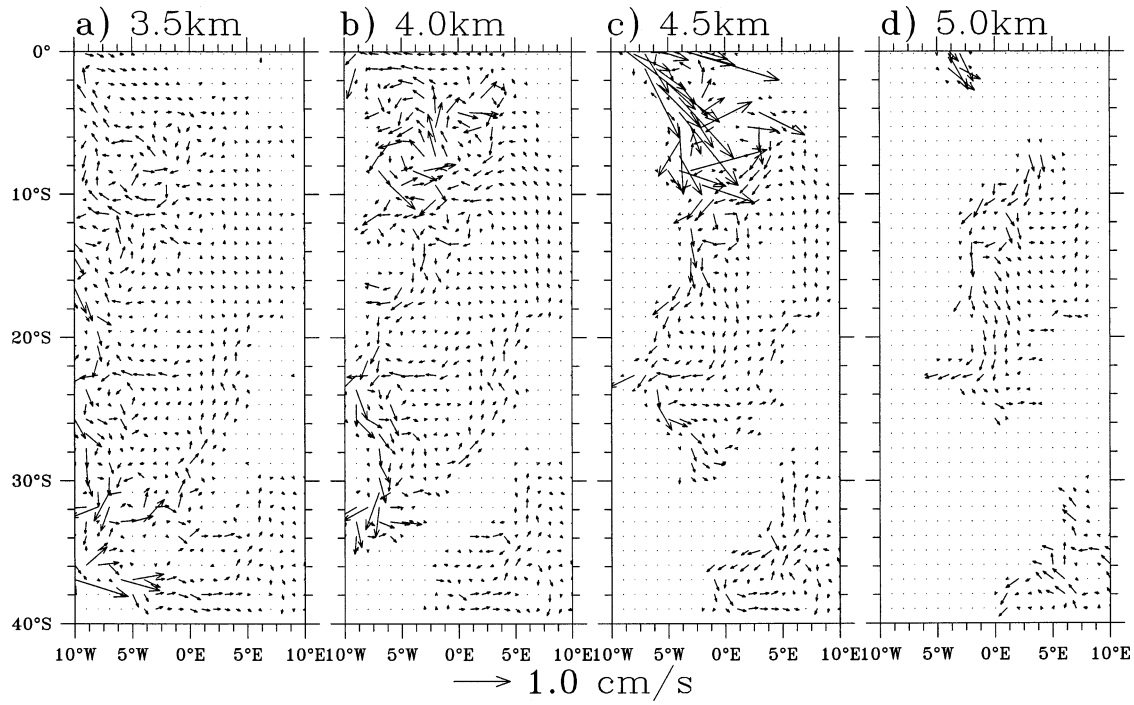

FIG. 4. Horizontal velocity within the Angola Basin at different levels for case A.

ridge in case C is much weaker than in case A, as shown in Figs. 3c and 3d.

The circulation in the Angola Basin is driven by the flow of deep water through the Romanche Fracture Zone, as shown by the strong inflow in the upper left corner in Fig. 4c. Strong mixing over the eastern slope of the midocean ridge induces a southward flow in the Angola Basin. Away from the ridge the flow is mostly equatorward; thus, the circulation in the Angola Basin is generally anticlockwise, opposite to the classical Stommel–Arons theory.

In order to quantify the horizontal circulation in these two deep basins, we calculated the northward mass flux, which is set to zero along the eastern boundary of each sub-basin and integrated westward over depth from 3.7 to 5.5 km. In the eastern part of the Angola Basin the flow is equatorward, with a total mass flux of about 0.36 Sv (Table 1), and in the western part of the Angola Basin the flow is poleward, carrying a mass flux of about 0.8 Sv. In the Brazil Basin the flow is generally equatorward, except in the middle of the basin, and the maximum mass flux is about 2.87 Sv. The meridional mass fluxes in cases B and C are slightly smaller (Table 1).

The mixing parameterization also affects the strength of the shallow and deep meridional overturning cells. Apparently, the simple scaling law for the strength of the meridional overturning rate does not apply to the present model because of the sponge layers along the northern and southern boundary and the inhomogeneous mixing rate. Nevertheless, strong mixing in the upper ocean induces a slightly larger meridional overturning rate of 17 Sv for case C as compared to 15 Sv for all

TABLE 1. Northward mass flux (sv) associated with the deep vertical overturning cells (below 3.25 km), shallow cell (above 3.25 km), and the horizontal gyres (integrated over depth 3.7–5.5 km)

	Case			
	A	B	C	D
	K			
	0.1–10	0.1	0.8451	0.1–10–1000
South Atlantic (shallow cell)	15.00	15.03	17.00	15.00
Brazil Basin (deep cell)	3.32	2.46	2.86	5.70
Angola Basin (deep cell)	−1.10	−0.64	−0.82	−1.66
South Atlantic (deep cell)	2.54	2.24	2.43	4.54
Brazil Basin (horizontal gyre)	2.87	2.27	2.58	4.99
Angola Basin (horizontal gyre)	0.36	0.25	0.28	0.17

other cases with a uniformly low mixing rate in the upper ocean. A strong meridional cell in case C also can be seen from the slightly stronger surface western boundary current at the 1.5-km level (Fig. 3a).

In order to compare the deep meridional circulation in these experiments, we search for the maximum (minimum) of meridional mass flux below 3.25 km in each sub-basin. In case A, the maximum northward mass flux associated with the deep cell is 3.32 Sv, which is larger than that of case B (2.46 Sv) and case C (2.86 Sv). The poleward mass flux associated with the deep cell in the Angola Basin is 1.10 Sv for case A, but it is only 0.64 Sv for case B and 0.82 Sv for case C.

Similar to the case of a meridional overturning cell in the upper ocean, strong mixing near the Romanche Fracture Zone (case D) induces a strong deep meridional cell, and draws more water into the Angola Basin. Note that the strength of the deep overturning cells in both the Brazil Basin and Angola Basin intensifies (Table 1). Therefore, localized strong mixing associated with overflows can affect the far field of the deep circulation.

b. Circulation in meridional sections

The circulation in the upper 2 km in the Brazil Basin is dominated by an anticlockwise wind-driven gyre, as shown by a section through 26°W (Fig. 5). Note that the westward branch of the subtropical gyre actually penetrates all the way to the seafloor around 25°S.

In the deep basin the vertical velocity is dominated by downwelling at this section. Strong downwelling in the basin interior is linked to the vertical gradient of diapycnal mixing rate; this will be discussed shortly. In addition, both the zonal and vertical velocity have alternating patterns, and such an alternating velocity pattern is not inconsistent with the direct measurements of deep circulation by Hogg and Owens (1999). The reason for such patterns is not very clear at this time. It is speculated that such alternating velocity patterns are due to the nonuniformity of the ridge topography. In addition, the diapycnal mixing rate can vary greatly along the axis of the ridge, thus inducing alternating velocity fields. The meridional circulation is equatorward for the upper 2 km but is poleward below 2 km, and there are a few patches of equatorward flow near the seafloor (Fig. 5b). Thus, the meridional circulation in the deep basin interior consists of a northward flow at the bottom and a southward return flow at shallower levels.

The circulation in the deep Angola Basin is slightly different. At 4 km, there is an anticlockwise abyssal gyre in the horizontal plane (Fig. 6a) and the meridional circulation in this section is clockwise (Figs. 6b,c). Such a circulation is induced by the cold water flowing southward through the Romanche Fracture Zone that fills up the basin through an anticlockwise gyre. The upwelling feeds the northward return flow and thus completes the circulation.

Warren and Speer (1991) discussed the circulation in

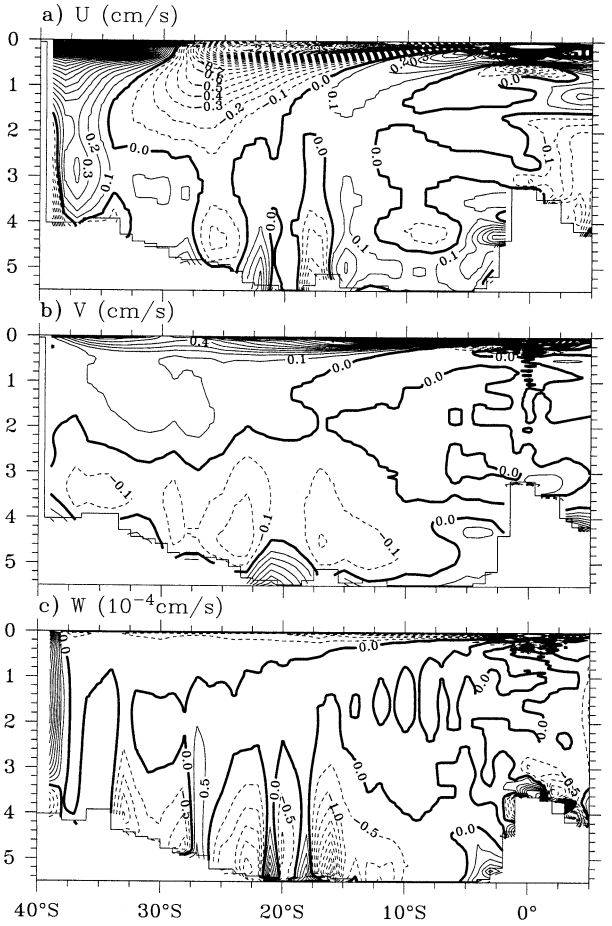

FIG. 5. Velocity field at 26°W (through the center of the Brazil Basin), depth in km: (a) zonal velocity (0.01 m s^{-1}); (b) meridional velocity (0.01 m s^{-1}); (c) vertical velocity (10^{-6} m s^{-1}).

the Angola Basin. Based on the classical theory of Stommel and Arons, they argued that the observations available at that time can be interpreted in terms of the Stommel–Arons theory. However, our numerical experiment indicates that the circulation can be more appropriately interpreted in terms of a non-Stommel–Arons circulation.

c. An index for the deviation from the Stommel–Arons circulation

Forty years ago, Stommel and Arons (1960) proposed the first theoretical model for the abyssal circulation. They began with a highly idealized model for the deep circulation by assuming 1) deep water originates from isolated point sources, 2) upwelling is uniform basin-wide, and 3) no bottom topography. From these assumptions, they showed that there should be western boundary currents and poleward flow in the ocean interior. Although the existence of the deep western boundary currents predicted by their theory has been largely confirmed by observations, the poleward flow

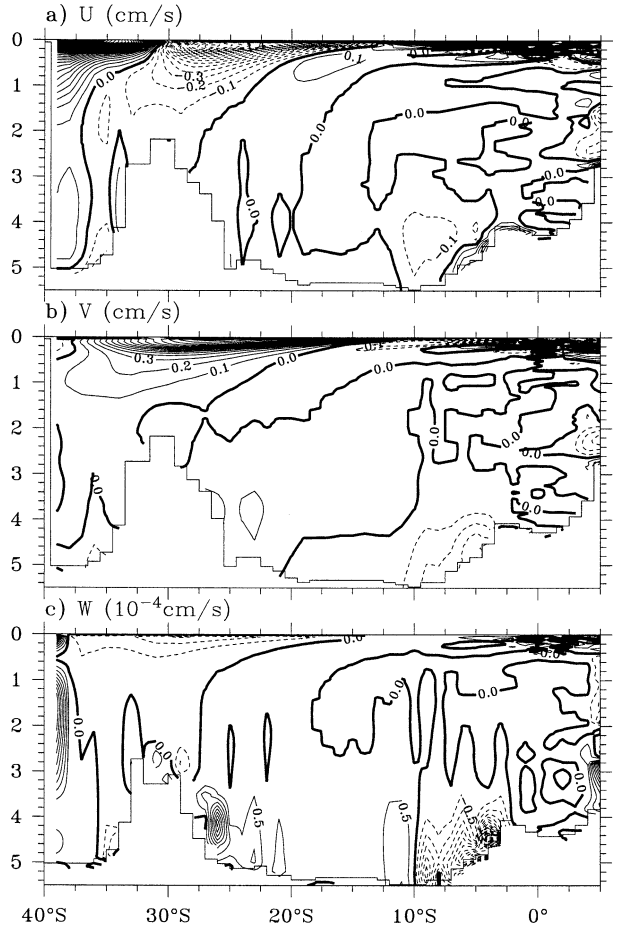

FIG. 6. Velocity field at 2°E (through the center of the Angola Basin), depth in km: (a) zonal velocity (0.01 m s^{-1}); (b) meridional velocity (0.01 m s^{-1}); (c) vertical velocity (10^{-6} m s^{-1}).

in the ocean interior predicted by their theory cannot be verified from observations. Through observations, and theoretical and numerical studies over the past decades, it is now evident that bottom topography and bottom-intensified mixing may play very important roles in controlling the potential vorticity balance and thus the abyssal circulation.

First of all, the assumption of basinwide uniform upwelling is not appropriate for the deep circulation. As Phillips et al. (1986) pointed out, boundary mixing can induce not only uphill flow, but also a tertiary flow perpendicular to the slope. The three-dimensional flows induced by bottom-intensified mixing have been discussed by many investigators (e.g., Garrett 1991; Cummins and Foreman 1998). In the present case, the tertiary flow appears in the form of upwelling near the midocean ridge and downwelling in the basin interior.

In order to illustrate this point, we introduce a vertical cycling index, which is defined as

$$V_c(z) = \mathrm{sgn}(W_p + W_n)\frac{\min(W_p, |W_n|)}{\max(W_p, |W_n|)} \times 100\%, \quad (4)$$

where W_p is the basin-integrated upwelling rate and W_n is the basin-integrated downwelling rate.

Stommel and Arons assumed a uniform upwelling, so $W_n = 0$; thus $V_c = 0$ for their model. On the other hand, $V_c = 100$ corresponds to the case with pure vertical recycling with no net flux through a given level; such a case is the theoretical limit of the non-Stommel–Arons circulation. In the oceans both upwelling and downwelling exist at any given depth, so V_c is normally nonzero. In fact, for most cases V_c is far from being zero. For example, in the Brazil Basin, V_c is close to either 100 or -100, indicating that there is a strong recirculation in the vertical direction, Fig. 7. As an example, in case A and at the depth of 4 km the upwelling branch carries 5.39 Sv and the downwelling branch carries 4.62 Sv, so the net upwelling rate is 0.78 Sv, which is fed from the AABW flux through the Vema Channel. There is also a large amount of mass flux through the side boundaries.

At depths below 4 km, the net upwelling rate is primarily controlled by the amount of mass flux of the AABW through the Vema Channel, so it is not very sensitive to the choice of diapycnal mixing rate; however, the strength of upwelling and downwelling depends on the choice of diapycnal mixing rate quite sensitively, as shown in Fig. 7. In fact, the upwelling branch in case A is the strongest, indicating a vigorous vertical cycling of water in the Brazil Basin. In comparison, the vertical cycling of water in case C is the weakest.

The choice of diapycnal mixing affects not only the deep circulation, as we have shown; it also affects the vertical upwelling rate over the whole depth range. This can been seen from the net upwelling rate in the Brazil Basin (Fig. 7). For example, there is a net upwelling at the depth range of 2–3 km for both case A and B; however, there is a net downwelling for case C at this depth range.

The difference in vertical net upwelling rate is directly related to the horizontal velocity field, indicating that the Ekman pumping effect due to the surface wind stress curl in the subtropical basin penetrates quite deep for case C. In comparison, the penetration of the Ekman pumping is much shallower for both case A and B. This difference is reflected in the depth of the main thermocline and the depth of the subtropical meridional cell. It is well known that a model with such a strong diapycnal mixing rate gives rise to a solution with a thermocline too deep and too diffusive; thus, the circulation in the upper ocean obtained from case C is not realistic.

The vertical mass flux profiles in the Angola Basin are much more sensitive to the choice of the diapycnal mixing rate, Fig. 8. The reason for this sensitivity is that the Angola Basin is primarily fed by water from the western basin through the Romanche Fracture Zone. As a result, water mass properties and the volume flux in the Angola Basin are the end product of mixing and circulation in the Brazil Basin. Therefore, the choice of

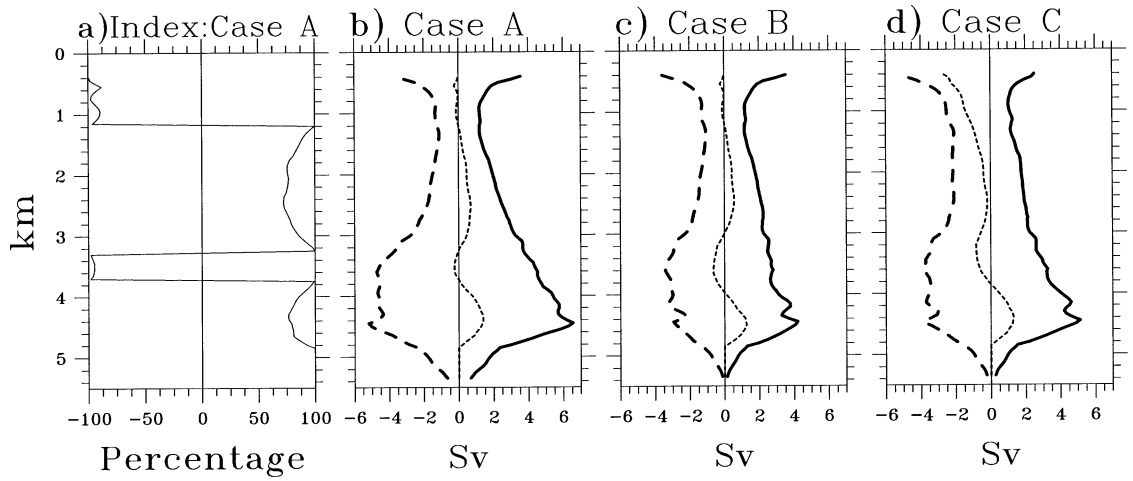

FIG. 7. Vertical mass flux profiles in the Brazil Basin; the solid line is for the total upwelling, the dashed line is for the total downwelling, and the thin dotted line is for the net vertical mass flux. (a) The vertical cycling index; the fluxes are shown for (b) case A, (c) case B, and (d) case C.

mixing parameterization in the Brazil Basin affects the model's circulation in the Angola Basin.

For example, at a depth of 3.5 km, the net downwelling rate is about 0.8 Sv for both case A and C, but it is less than 0.2 Sv for case B. Above this depth the net vertical mass flux rate is quite different for all three cases, indicating that the circulation pattern in the Angola Basin is rather sensitive to the choice of diapycnal mixing rate. Finally, we note that there is also a very vigorous vertical cycling of water in the Angola Basin, as indicated by the vertical cycling index shown in Fig. 8a.

d. Properties on zonal sections

For a close examination of the solutions, we plot temperature and velocity (below 2 km) for different zonal sections. (The salinity gradient is rather weak for the deep basin, so maps of salinity are less informative and are not included here.) First, we describe the structure of the circulation obtained for cases A, B, and C at 19°S, Figs. 9 and 10. The isothermal contours obtained from case A have many important features.

1) In the Brazil Basin there is clearly the abyssal thermocline around the potential temperature range of 0.8°–2.0°C.
2) On both sides of the midocean ridge, isotherms dive toward the ridge and seem more ''perpendicular'' to the local slope, consistent with the theory of a bottom boundary layer with an isolating condition (e.g., Phillips 1970; Wunsch 1970).
3) Isotherms in the Brazil Basin interior slope downward to the east.

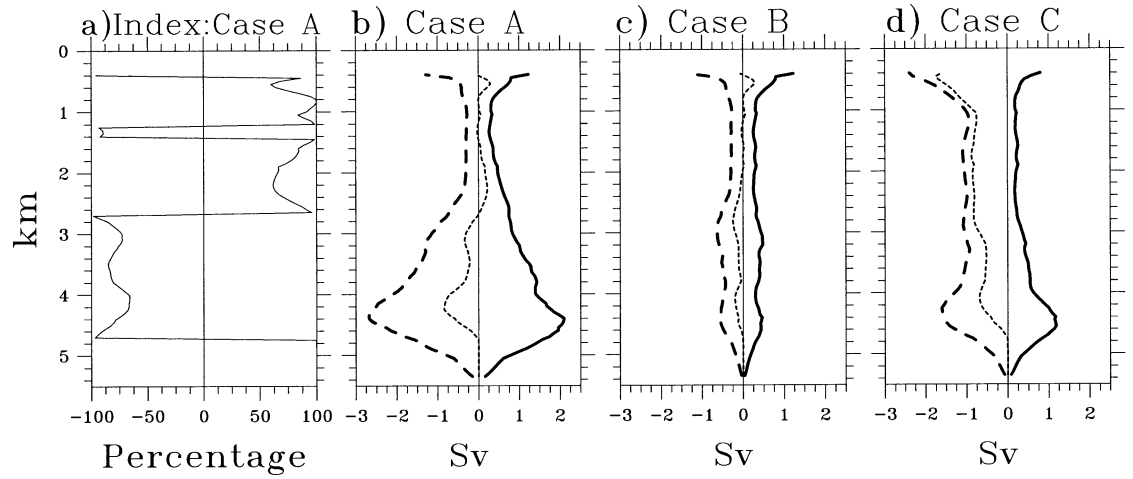

FIG. 8. Vertical mass flux profiles in the Angola Basin; the solid line is for the total upwelling, the dashed line is for the total downwelling, and the thin dotted line is for the net vertical mass flux. (a) The vertical cycling index for case A; the fluxes are shown for (b) case A, (c) case B, and (d) case C.

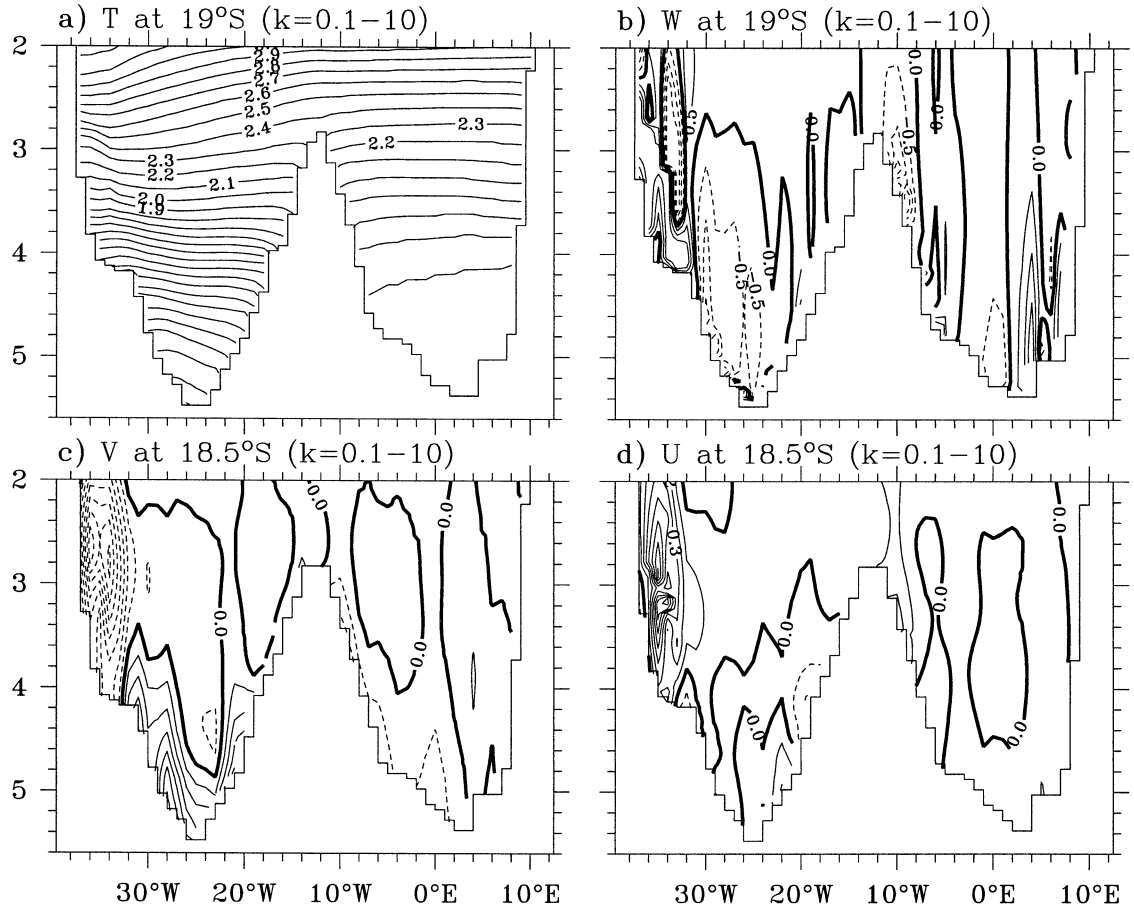

FIG. 9. Circulation at 19°S for case A (depth in km). (a) Potential temperature (°C); (b) vertical velocity (10^{-6} m s^{-1}); (c) meridional velocity (0.01 m s^{-1}, contour interval 0.001 m s^{-1}); (d) zonal velocity (0.01 m s^{-1}).

Note that these features are all consistent with the observations taken from many cross-basin hydrographic sections. The isothermal contours shown in Fig. 9 closely resemble the World Ocean Circulation Experiment (WOCE) hydrographic section taken along 19°S, as described by Siedler et al. (1996). In particular, the location and slope of the deepest contour, $\theta = 0.3$°C, are very close to the corresponding isotherm from the WOCE 19°S section.

In the Brazil Basin water flows eastward below 4.5

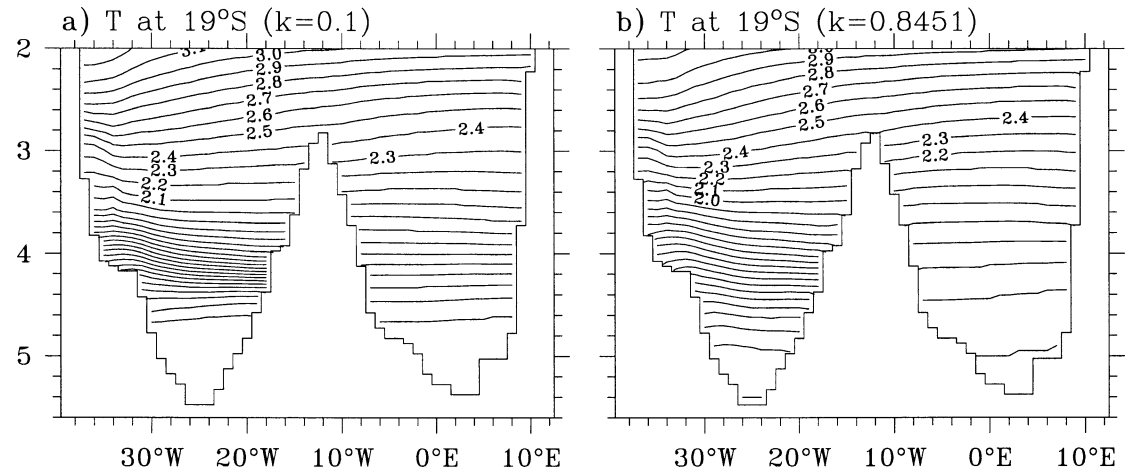

FIG. 10. Potential temperature (°C) at 19°S for case B and C (depth in km).

km (Figs. 9d and 9b); this eastward and uphill flow over the bottom topography is primarily induced by the strong bottom-intensified mixing over the ridge. However, the flow direction reverses above 4.5 km; a generally westward flow occurs between 3.7 and 4.5 km—not inconsistent with the circulation pattern inferred from deep floats (Hogg and Owens 1999). In the Angola Basin there are actually two zonal cells rotating in opposite directions. In the eastern part, there is an anticlockwise circulation with a mass flux of more than 0.3 Sv. This cell consists of eastward flow over the seafloor and the westward return flow at the depth of 4–4.5 km. In the western part, there is a weak clockwise circulation with a slow uphill flow over the eastern slope of the midocean ridge, apparently induced by the strong bottom-intensified mixing there. However, the strength of the upward motion along the eastern slope is much weaker than the corresponding upward motion along the western slope of the midocean ridge. Thus, the circulation in the zonal section is similar to the case discussed by Cummins and Foreman (1998) for the flow induced by bottom-intensified mixing over a seamount.

The relatively steep isothermal contours indicate a relatively strong bottom boundary current along both sides of the midocean ridge, as shown in Fig. 9c. There the associated zonal and vertical velocities are also stronger, compared with cases B and C (figures not included). Note that the bottom-intensified mixing rate induces upwelling over the western slope of the midocean ridge and downwelling over the lower part of the ridge (Fig. 9b). This is similar to the flow pattern inferred from the tracer distribution observations in the deep Brazil Basin (St. Laurent et al. 2001). This can be explained as follows. Using a one-dimensional model as a crude approximation for density conservation, the basic balance is

$$w = \kappa_z + \kappa \frac{\rho_{zz}}{\rho_z}. \tag{5}$$

For the model with bottom-intensified mixing in case A, the first term on the right-hand side is on the order of $\kappa_z \approx -2 \times 10^{-6}$ m^2 s^{-1}, so it is a substantial contribution to the downwelling near the outer part of the midocean ridge. Due to the continuity conservation, this downwelling should enhance the upwelling near the axis of the midocean ridge, where the second term on the right-hand side of (5) is positive due to an almost zero density gradient near the seafloor. In comparison, for cases B and C the κ_z term is identically equal to zero, so there is no downwelling near the bottom of the midocean ridge.

Note that isotherms obtained from cases B and C are mostly flat near the midocean ridge and in the basin interior (Figs. 10a,b). The lowest temperatures are 0.1°C for case B and 0.2°C for case C, which is clearly too cold compared with observations. Note that the abyssal thermocline is reproduced in all three cases, although the temperature gradient in cases B and C seems too strong in comparison with observations, indicating that mixing is not strong enough for these two cases. The resulting isothermal slope suggests a rather slow bottom boundary current associated with the density field.

In the Angola Basin the coldest water is in the eastern part of the seafloor. The deep water in all three experiments is too cold, indicating that mixing is not strong enough, with case B being the worst and case A slightly better among the three. There may be sources of the missing mixing: First, there is strong mixing in the Romanche Fracture Zone. Second, mixing in the Angola Basin may be different from that in the Brazil Basin. Since there are no direct measurements available for the Angola Basin, we will assume that the missing intensified mixing in the Romanche Fracture Zone might be the source of too-cold water in the model.

As an effort to improve the model simulation, we carried out a fourth experiment, case D, with a localized intensified mixing of 0.1 m^2 s^{-1}. The results from this experiment show a substantial improvement of temperature simulation for the deep water in the Angola Basin, Fig. 11. In the Brazil Basin the largest temperature change, 0.16°C, is at 4.5 km and on the middle of slope, but in the Angola Basin it is 0.22°C and on the seafloor. On the other hand, temperature at the middle level, 2–3.5 km, is slightly colder. Changes in meridional velocity induced by this temperature change are shown in Fig. 11b. As discussed above, localized mixing can affect the circulation and water properties both downstream and upstream.

The structure of the solution has similar features at other sections. Here we discuss a section at 5°S obtained from case A, Fig. 12. The solution at this section looks similar to that at 19°S; however, it is much more complicated in detail. The most important difference is that now the coldest water in the Angola Basin is located in the western half of the basin, which is different from the section at 19°S. This patch of cold water is associated with the poleward flow directly from the source water, as indicated by the negative meridional velocity in Fig. 12b. Near the top of the midocean ridge, the bottom boundary current on both sides of the ridge actually moves equatorward. Thus, our model provides a dynamic interpretation for the bottom water temperature with a circulation that is opposite to the classical Stommel–Arons theory; nevertheless, everything is self-consistent within the dynamic framework.

e. Mass flux of boundary currents

The most important feature of the model is the deep meridional overturning cell associated with the AABW flux, which is defined for water going through the Vema Channel with potential temperature cooler than 1°C. Due to the limitation of the horizontal resolution used in this model, the Vema Channel is represented by two rows of grids with a depth of 4.6 km. Although this 2° channel

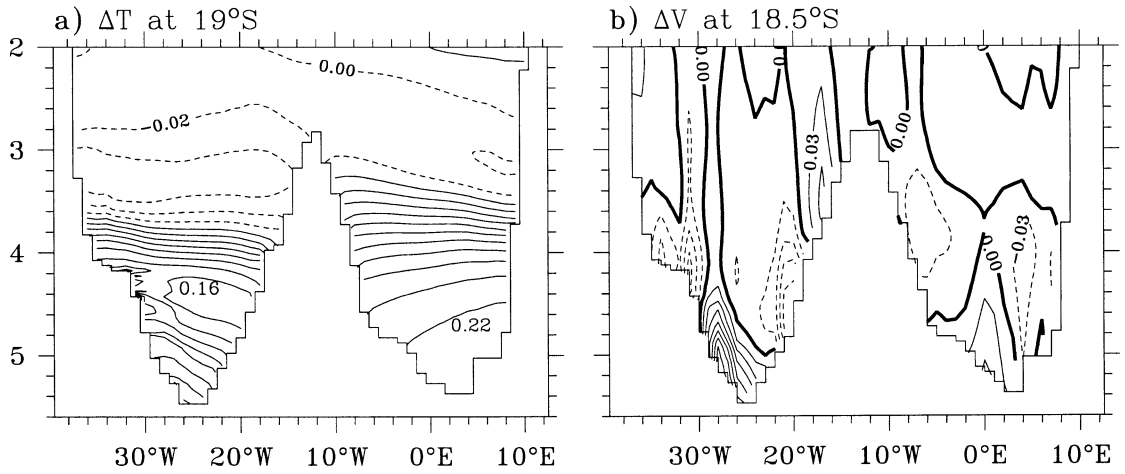

FIG. 11. Difference of the circulation (case D − case A) at 19°S (depth in km). (a) Potential temperature (°C); (b) meridional velocity (0.01 m s^{-1}).

is much wider than the real channel, the mass flux through this channel in our model is only about 2 Sv (Table 2), smaller than the value of 4 Sv obtained from field observations (Hogg et al. 1996). This flux is primarily controlled by the model geometry and the water mass properties specified along the southern boundary of the model ocean, so it does not vary with the mixing parameterization in each case, as shown in the first row in Table 2.

On the other hand, the mass fluxes along the eastern boundary and western boundary of the Brazil Basin vary greatly, depending on the mixing parameterization used in each case (Table 2). In this table WSCR is defined as the mass flux of northward current adjacent to the western slope of the midocean ridge (22°–15°W) in the depth range of 3–5 km; BWBC is defined as the mass flux of the northward current adjacent to the western boundary of the basin (34°–26°W) below 3.5 km; and DWBC is defined as the mass flux of the southward current adjacent to the western boundary of the basin (38°–32°W) over the depth range of 1.5–4.5 km.

From Table 2, it is readily seen that bottom-intensified mixing over the midocean ridge intensifies the boundary current along the midocean ridge, and it also causes a decline of mass flux of the bottom western boundary current. At the same time the mass flux of the deep western boundary current also increases. In comparison, the mass flux of the boundary current along the western slope of the midocean ridge for cases B and C is substantially smaller than in case A. As discussed above, we are aware of the artificial mixing due to the advection in the *z*-coordinate model. Since diapycnal mixing for the western part of the Brazil Basin is the same for case A and case B, the difference in circulation between these two cases clearly demonstrates the dynamic effects of bottom-intensified mixing. When strong and localized mixing in the Romanche Fracture Zone is included, the influence is not confined to downstream. In fact, the

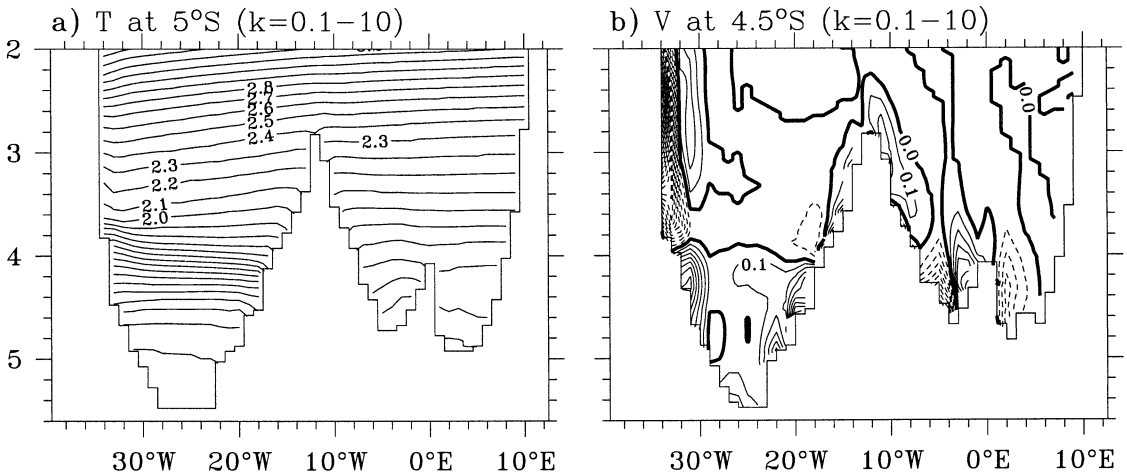

FIG. 12. Circulation at 5°S for case A (depth in km). (a) Potential temperature (°C); (b) meridional velocity (0.01 m s^{-1}).

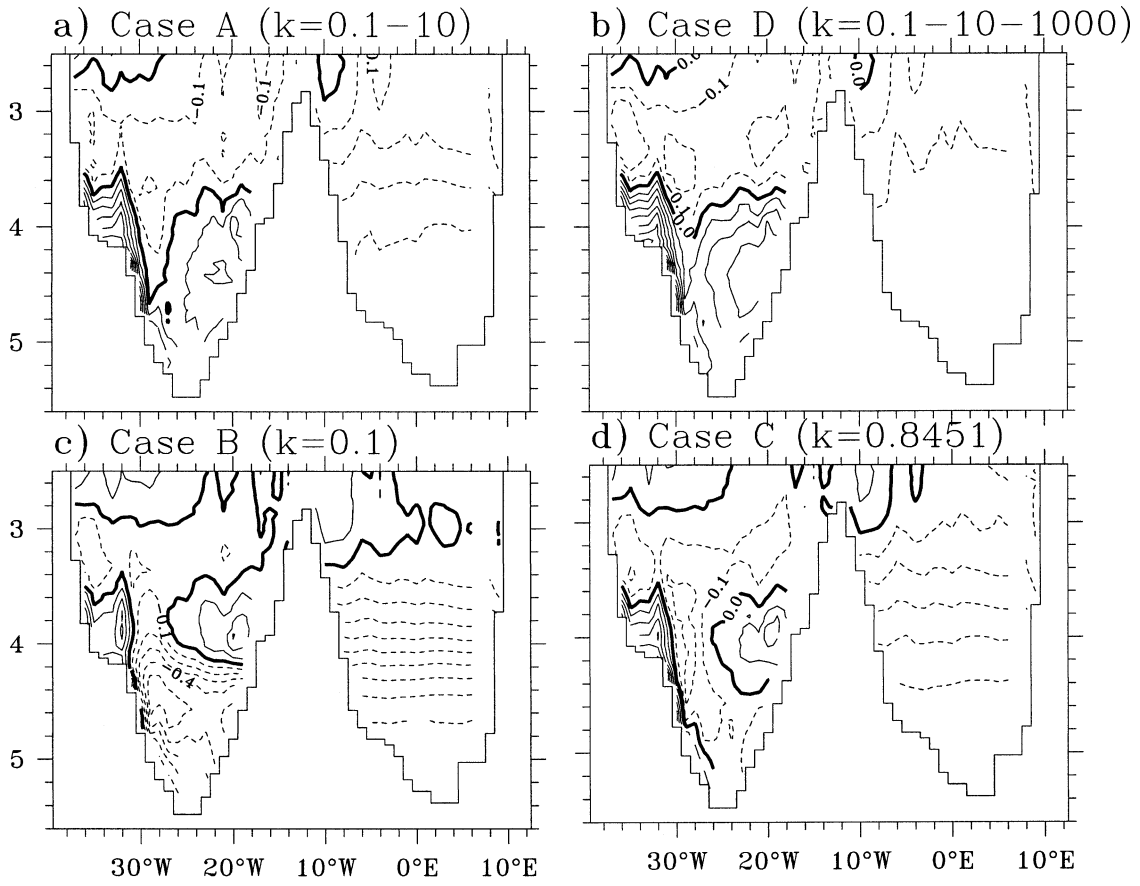

FIG. 13. Difference in potential temperature at 19°S (model − WOCE) (°C; depth in km).

influence is also very strong upstream, as shown in Fig. 11. Second, the WSCR in case D is stronger than in case B and C, but it is weaker than in case A, because intensified mixing creates less geostrophic shear for the deep ocean, as shown in Fig. 11.

f. Comparison with the WOCE 19°S section

As a final step in examining the solutions, we plotted the difference in potential temperature between all four cases and the corresponding WOCE section along 19°S, Fig. 13. In the Brazil Basin deep water temperature near the western boundary is too warm for all four cases, indicating that the model's deep western boundary is too weak, so there is not enough cold water within the boundary layer. This is related to the fact that the model's horizontal resolution is rather low, so it does not resolve the western boundary current accurately.

In the interior of the Brazil Basin, deep water in case A and D is slightly too warm, but in case B and C it is too cold, indicating that mixing in the first two cases may be too strong and it is too weak in the last two cases. It is noted that there is a positive error at depth 4 km on the western slope of the midocean ridge for all cases. The source of such a systematic error is unclear at this time. We speculate that such errors may be induced through relaxation to the Levitus climatology at the sponge layer along the southern boundary of the model ocean.

In the Angola Basin deep water is too cold for all cases, indicating that mixing is not strong enough for all cases. It is clear that intensified mixing added in the vicinity of the Romanche Fracture Zone does improve

TABLE 2. Mass flux of different currents in the Brazil Basin (Sv). AABW: Antarctic Bottom Water through the Vema Channel (30.5°S), WSCR: western slope current along the ridge, BWBC: bottom western boundary current and DWBC: deep western boundary current. Except for AABW, all other fluxes are defined at 18.5°S.

	Case			
	A	B	C	D
	K			
	0.1–10	0.1	0.8451	0.1–10–1000
AABW	2.11	1.91	2.10	2.18
WSCR	0.57	0.19	0.26	0.35
BWBC	1.36	1.87	1.86	1.43
DWBC	−4.14	−4.14	−3.53	−4.07

the model's temperature simulation in the Angola Basin greatly; however, temperature in the deep Brazil Basin is also increased. Over all, mixing distribution in case D seems the best among the four cases; however, a mixing scheme that produces the best fit to observation in the South Atlantic remains a challenge.

4. Conclusions

Our numerical experiments based on a *z*-coordinate model indicate that with realistic bottom topography the abyssal circulation deviates from the classical Stommel–Arons circulation pattern noticeably, even for the case with uniformly weak mixing. For the case with strong bottom-intensified mixing over the midocean ridge, the circulation departs from the classical Stommel–Arons circulation remarkably. Our results are consistent with many previous studies, such as the boundary mixing theory summarized by Garrett (1991), the numerical study by Cummins and Foreman (1998), and the theoretical study by Spall (2001). In summary, our results demonstrate the vitally important dynamic role of bottom topography in controlling the deep circulation.

Our study is only a small step in understanding the dynamical meaning of nonuniform mixing, and much effort is required in order to fully understand its impact. In order to simulate the deep circulation and water mass properties, it seems very crucial to

1) treat the bottom topography accurately. It is of vital importance to have the deep channels between different sub-basins connected for low-resolution models.
2) use the best estimate for the mixing rate. A spatially varying mixing rate is clearly one of the most critical parts of ocean models for simulating the deep circulation. In particular, extremely strong localized mixing associated with overflow through sills connecting different basins has been omitted in most previous basin-scale simulations; however, such strong localized mixing may be vitally important in simulating the deep circulation accurately.
3) include the geothermal heat flux. Geothermal heat flux can be an important contributor to the abyssal stratification, as demonstrated by Thompson and Johnson (1996). Recently, Adcroft et al. (2001) have carried out a numerical experiment using an oceanic general circulation model. By including a uniformly distributed geothermal heat flux of 50 mW m^{-2}, the bottom temperature increases by 0.3°C, compared with the case of no geothermal heat flux. Such a change in bottom water temperature is substantial; thus, it is clear that if we want to simulate the bottom water properties and circulation accurately, including the geothermal heat flux is a must.

Acknowledgments. We thank Drs. Nelson Hogg and Ray Schmitt for their suggestions and physical insights about the deep circulation. This study was supported by the National Science Foundation through Grant OCE-0094807 to the Woods Hole Oceanographic Institution.

REFERENCES

Adcroft, A., J. R. Scott, and J. Marotzke, 2001: Impact of geothermal heating on the global ocean circulation. *Geophy. Res. Lett.,* **28,** 1735–1738.

Bryan, F., 1987: Parameter sensitivity of primitive equation ocean general circulation models. *J. Phys. Oceanogr.,* **17,** 970–985.

Bryan, K., and L. J. Lewis, 1979: A water mass model of the world ocean. *J. Geophys. Res.,* **84,** 2503–2517.

Cummins, P. F., and M. G. G. Foreman, 1998: A numerical study of circulation driven by mixing over a submarine bank. *Deep-Sea Res. I,* **45,** 745–769.

de Madron, D., and G. Weatherly, 1994: Circulation, transport and bottom boundary layers of the deep currents in the Brazil Basin. *J. Mar. Res.,* **52,** 583–638.

Garrett, C., 1991: Marginal mixing theories. *Atmos. Ocean,* **29,** 313–339.

——, P. MacCready, and P. Rhines, 1993: Boundary mixing and arrested Ekman layers: Rotating stratified flow near a sloping boundary. *Annu. Rev. Fluid Mech.,* **25,** 291–323.

Griffies, S. M., R. C. Pacanowski, and R. W. Hallberg, 2000: Spurious diapycnal mixing associated with advection in a *z*-coordinate ocean model. *Mon. Wea. Rev.,* **128,** 538–564.

Ferron, B., H. Mercier, K. Speer, A. Gargett, and K. Polzin, 1998: Mixing in the Romanche Fracture Zone. *J. Phys. Oceanogr.,* **28,** 1929–1945.

Hellerman, S., and M. Rosenstein, 1983: Normal monthly wind stress over the world ocean with error estimates. *J. Phys. Oceanogr.,* **13,** 1093–1104.

Hogg, N. G., and W. B. Owens, 1999: Direct measurement of the deep circulation within the Brazil Basin. *Deep-Sea Res. II,* **46,** 335–353.

——, P. Biscaye, W. Gardner, and W. J. Schmitz Jr., 1982: On the transport and modification of Antarctic Bottom Water in the Vema Channel. *J. Mar. Res.,* **40** (Suppl.), 231–263.

——, W. B. Owens, G. Siedler, and W. Zenk, 1996: Circulation in the Deep Brazil Basin. *The South Atlantic: Present and Past Circulation,* G. Wefer et al., Eds., Springer-Verlag, 249–260.

Ledwell, J. R., E. T. Montgomery, K. L. Polzin, L. C. St. Laurent, R. W. Schmitt, and J. M. Toole, 2000: Evidence for enhanced mixing over rough topography in the abyssal ocean. *Nature,* **403,** 179–182.

Levitus, S., and T. P. Boyer, 1994: *Temperature.* Vol. 4, *World Ocean Atlas 1994,* NOAA Atlas NESDIS 4, 117 pp.

——, R. Burgett, and T. P. Boyer, 1994: *Salinity.* Vol. 3, *World Ocean Atlas 1994,* NOAA Atlas NESDIS 3, 99 pp.

Marotzke, J., 1997: Boundary mixing and the dynamics of three-dimensional thermohaline circulations. *J. Phys. Oceanogr.,* **27,** 1713–1728.

Morris, M. Y., M. M. Hall, L. C. St. Laurent, and N. G. Hogg, 2001: Abyssal mixing in the Brazil Basin. *J. Phys. Oceanogr.,* **31,** 3331–3398.

Pacanowsky, R. C., 1995: MOM2 documentation user's guide and reference manual, version 2. GFDL Ocean Tech. Rep. 3, 232 pp.

Phillips, O. M., 1970: On flows induced by diffusion in a stable stratified fluid. *Deep-Sea Res.,* **17,** 435–443.

——, J. Shyu, and H. Salmun, 1986: An experiment on boundary mixing: Mean circulation and transport rates. *J. Fluid Mech.,* **173,** 473–499.

Polzin, K. L., K. G. Speer, J. M. Toole, and R. W. Schmitt, 1996: Intense mixing of Antarctic Bottom Water in the equatorial Atlantic Ocean. *Nature,* **380,** 54–57.

——, J. M. Toole, J. R. Ledwell, and R. W. Schmitt, 1997: Spatial

variability of turbulent mixing in the abyssal ocean. *Science*, **276,** 93–96.
Samelson, R. M., 1998: Large-scale circulation with localized enhanced vertical mixing. *J. Phys. Oceanogr.*, **28,** 712–726.
Siedler, G., T. J. Muller, R. Onken, M. Arhan, H. Mercier, B. A. King, and P. M. Saunders, 1996: The zonal WOCE sections in the South Atlantic. *The South Atlantic: Present and Past Circulation*, G. Wefer et al., Eds., Springer-Verlag, 83–104.
Song, T., and Y. Chao, 2000: An embedded bottom boundary layer formulation for *z*-coordinate ocean models. *J. Atmos. Oceanic Tech.*, **17,** 546–560.
Spall, M. A., 2001: Large-scale circulations forced by localized mixing over a sloping bottom. *J. Phys. Oceanogr.*, **31,** 2369–2384.
St. Laurent, L. C., J. M. Toole, and R. W. Schmitt, 2001: Buoyancy forcing by turbulence above rough topography in the abyssal Brazil Basin. *J. Phys. Oceanogr.*, **31,** 3476–3495.
Stommel, H., and A. B. Arons, 1960: On the abyssal circulation of the world ocean—I. Stationary planetary flow patterns on a sphere. *Deep-Sea Res.*, **6,** 140–154.
Thompson, L., and G. C. Johnson, 1996: Abyssal currents generated by diffusion and geothermal heating over rises. *Deep-Sea Res.*, **43,** 193–211.
Warren, B. A., and K. G. Speer, 1991: Deep circulation in the eastern South Atlantic Ocean. *Deep-Sea Res.*, **38** (Suppl.), 281–322.
Wunsch, C., 1970: On oceanic boundary mixing. *Deep-Sea Res.*, **17,** 293–301.
Yang, J., and J. Price, 2000: Water-mass formation and vorticity balance in an abyssal ocean circulation. *J. Mar. Res.*, **58,** 789–808.